Published in final edited form as:
J Am Chem Soc. 2013 November 6; 135(44): . doi:10.1021/ja408917n.

Picomolar Inhibitors of HIV Reverse Transcriptase Featuring Bicyclic Replacement of a Cyanovinylphenyl Group

Won-Gil Lee[†], **Ricardo Gallardo-Macias**[†], **Kathleen M. Frey**[‡], **Krasimir A. Spasov**[‡], **Mariela Bollini**[†], **Karen S. Anderson**[‡,*], and **William L. Jorgensen**[†,*]

[†]Department of Chemistry, Yale University, New Haven, Connecticut 06520-8107

[‡]Department of Pharmacology, Yale University School of Medicine, New Haven, CT 06520-8066

Abstract

Members of the catechol diether class are highly potent non-nucleoside inhibitors of HIV-1 reverse transcriptase (NNRTIs). The most active compounds yield EC_{50} values below 0.5 nM in assays using human T-cells infected by wild-type HIV-1. However, these compounds like rilpivirine, the most recently FDA-approved NNRTI, bear a cyanovinylphenyl (CVP) group. This is an uncommon substructure in drugs that gives reactivity concerns. In the present work, computer simulations were used to design bicyclic replacements for the CVP group. The predicted viability of a 2-cyanoindolizinyl alternative was confirmed experimentally and provided compounds with 0.4-nM activity against the wild-type virus. The compounds also performed well with EC_{50} values of 10 nM against the challenging HIV-1 variant that contains the Lys103Asn/Tyr181Cys double mutation in the RT enzyme. Indolyl and benzofuranyl analogs were also investigated; the most potent compounds in these cases have EC_{50} values towards wild-type HIV-1 near 10 nM and high-nM activities towards the double-variant. The structural expectations from the modeling were much enhanced by obtaining an X-ray crystal structure at 2.88-Å resolution for the complex of the parent 2-cyanoindolizine **10b** and HIV-1 RT. The aqueous solubilities of the most potent indolizine analogs were also measured to be ca. 40 μg/ml, which is similar to that for the approved drug efavirenz and ca. 1000-fold greater than for rilpivirine.

INTRODUCTION

Inhibitors of HIV-1 reverse transcriptase are central to anti-HIV therapy.[1] Though there are five FDA-approved drugs in the non-nucleoside class,[2] efavirenz (**1**) and rilpivirine (**2**) are particularly important as they are components of the one-a-day combination therapies Atripla and Complera.[3] The other two components of the pills are the same, emtricitabine and tenofovir, which are in the nucleoside class of HIV-RT inhibitors. The goal of our research has been to discover new non-nucleoside inhibitors (NNRTIs) that may incorporate advantages for administration, formulation, diminished side effects, and activity towards variant strains of the virus. For example, issues with efavirenz include its daily dosage of 600 mg, poor activity towards HIV-1 variants containing the commonly occurring Lys103Asn (K103N) mutation in RT, and neurological side effects. The situation with

Corresponding Authors, william.jorgensen@yale.edu, karen.anderson@yale.edu.

The authors declare no competing financial interest.

ASSOCIATED CONTENT

Supporting Information

Synthetic details, NMR and HRMS spectral data for compounds in Tables 1, and crystallographic details. The crystal structure data for the complex of **10b** and HIV-RT have been deposited in the RCSB Protein Data Bank with the code 4MFB. These materials are available free of charge via the Internet at http://pubs.acs.org .

rilpivirine is curious. Although it has much superior performance in cell-based assays than efavirenz, more virological failure is observed for patients using Complera than Atripla. [3,4] Another unusual feature of rilpivirine is its extremely low aqueous solubility (0.02 μg/ml)[5] in comparison to the typical range of 4 – 4000 μg/ml for oral drugs.[6]

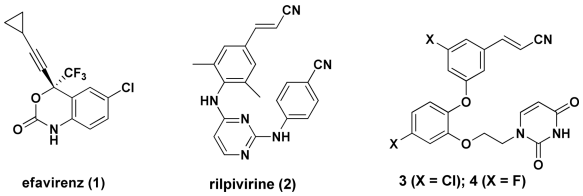

The challenges in developing new NNRTIs that represent an advance over existing compounds are great. One seeks simultaneously compounds that embody high potency towards the wild-type (WT) virus and numerous clinically observed variants, good pharmacological properties including solubility, an absence of structural features that may lead to rapid metabolism, and avoidance of toxicities stemming from reactive functional groups or metabolic products.[7,8] A particularly promising class of NNRTIs that we have developed is catechol diethers including **3** and **4**.[9] **3** appears to be the most potent anti-HIV agent ever reported with an EC_{50} of 0.055 nM in the standard MT-2 cell assay using wild-type HIV-1. The difluoro analog **4** is also extremely potent at 0.32 nM, has good potency towards variant strains containing the Y181C (16 nM) and K103N/Y181C (85 nM) mutations, and shows low cytotoxicity towards the T-cells (CC_{50} = 45 μM). It was also possible to obtain X-ray crystal structures of **3** and **4** in complex with WT HIV-RT.[10] Thus, further structure-based design activities in the catechol diether series have a firm foundation.

A structural feature in **3** and **4** as well as in rilpivirine that is addressed here is the cyanovinyl (CV) group. For most medicinal chemists viewing these structures, concern arises that the CV group may be sufficiently electrophilic to act as a “Michael acceptor” leading to potential covalent modification of proteins, nucleic acids, or other biological entities. Though in reality unsaturated nitriles are poor Michael acceptors that require reactive organometallic nucleophiles to undergo conjugate additions,[11] the fact is almost no approved drugs contain a cyanovinyl group, and lack of precedent is often taken as a warning sign in drug discovery. When a search is done for a C=C-C≡N substructure in a comprehensive file containing the structures of ca. 1900 approved oral drugs,[12] there are just five hits: rilpivirine, entacapone, nilvadipine, teriflunomide, and trilostane. For the latter two examples, the substructure only arises as a tautomer of an α-cyanoketone. Rilpivirine is unique in incorporating a simple CV group. By contrast, non-vinyl cyano groups are generally considered to be acceptable in drugs;[13] there are 36 examples in the database.

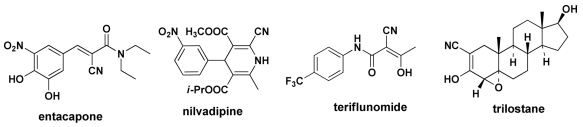

Thus, we set out to find a replacement for the cyanovinyl group in the catechol diethers. The prior results demonstrated the importance of the CV group to activity.[9] The analog of **3** with the CV group truncated to just cyano has an EC_{50} of 14 nM towards the WT virus, and other compounds with the cyano of the CV group replaced by chlorine, OCH_3, or $CONH_2$ showed 100 to 1000-fold losses in activity. These findings are consistent with the modeling and crystallography,[9,10] which document (a) close contact between the CV group and Trp229 in the NNRTI binding site, and (b) projection of the cyano group into the “tunnel” heading towards the polymerase active site with a water molecule hydrogen bonded to the cyano

nitrogen atom. In order to replace these features and keeping in mind space constraints, it was decided to consider 6:5 heterobicyclic possibilities as indicated by **5** and **6**. In **5**, R" would likely be cyano, while in **6** the azole nitrogen would retain a hydrogen bond accepting site for a water molecule. In both cases, the choice of heteroatoms in the five-membered ring for optimal interaction with Trp229 was not obvious, nor was the effect of loss of the torsional degree of freedom associated with the CV group. In view of the wide range of options and the anticipated synthetic challenges, guidance was sought from computational analyses, specifically free energy perturbation calculations to predict relative free energies of binding for many alternatives.

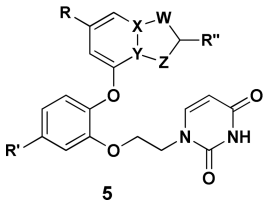

5

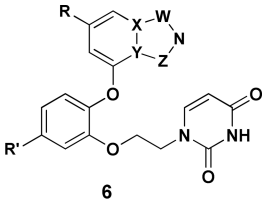

6

COMPUTATIONAL DESIGN

The computational procedures that were utilized are exactly the same as in earlier studies.[9,14] Starting from a crystal structure of the protein, the BOMB program[7] was used to build initial structures for the desired protein-ligand complexes. Conjugate-gradient energy minimizations were performed to relax the structures and Monte Carlo free-energy perturbation (MC/FEP) were carried out to compute relative free energies of binding. The calculations were performed with the MCPRO program[15] using the OPLS-AA force field for the protein,[16] OPLS/CM1A for the ligands,[17] and the TIP4P water model.[18] The FEP calculations used 11 windows of simple overlap sampling, and many were also checked using 14 windows of double-wide sampling.[19] The typical difference between the results was about 0.5 kcal/mol, which is a good measure of the statistical uncertainties. When both procedures were executed, the average of the results is reported. Each window covered at least 10 million configurations of equilibration and 10 million configurations of averaging. The unbound ligands and complexes were solvated in water caps with a 25-Å radius, amounting to ca. 2000 and 1250 water molecules, respectively. The 175 amino acid residues nearest to the ligand were included in the model for the complexes. A residue-based cutoff for non-bonded interactions was invoked at 10 Å. After short conjugate-gradient optimizations, the backbone atoms of the protein were not moved. The ligand and side chains with any atom within ca. 10 Å of the ligand were fully sampled. All water molecules were sampled using translations and rigid rotations.

The alternative heterocycles that were considered are designated **7a** – **7k** in Figure 1. They are typical 6:5 fused-ring possibilities, namely, indoles, indolizines, benzofurans, benzisoxazoles, and imidazopyridines. **7a, 7d, 7e**, and **7b** represent a 'nitrogen walk' around the 5-membered ring; the remaining isoindole isomer was excluded as such structures are labile.[20] Furthermore, benzothiophenes were not considered as they appeared less promising in initial structure building than the benzofurans, and they are both prone to have metabolic liabilities.[8] It was also anticipated that a substituent R" would be utilized as indicated in **5**, so the methylated analogs **7l** – **7r** were modeled.

The structural situation is exemplified for the complex of **7l** in Figure 2. The expectation from the modeling for **7a** – **7r** and the crystallography for **3** and **4**,[10] assuming **7l** would bind at all, is that the indole fragment would make π contacts face-to-face with Tyr188 and edge-to-face with Tyr181 and Trp229. In addition, the methyl group or another substituent at C2 would project below the Phe227-Leu228-Trp229 loop into the tunnel heading towards the

polymerase active site. The tunnel contains water molecules; however, the pocket below C3 of the indole is dry. Consequently, heterocycles with an unsaturated nitrogen in the C3 position, e.g., the benzimidazole corresponding to **7a** or benzoxazole corresponding to **7f**, were not considered. There is also no water in the small pocket between Pro95 and Tyr188. Thus, introductions of nitrogen atoms into the three possible sites for the six-membered ring were not evaluated.

The results of the MC/FEP calculations are summarized in Figure 1. Many of the perturbations were made from **7a**, which is taken as the reference compound for the listed relative free energies of binding, $\Delta\Delta G_b$. For methylated compounds, the perturbations were made to the desmethyl analog, e.g., **7m** to **7b**. One can attempt to rationalize the results after the fact, but even correct qualitative predictions in the absence of the computations are elusive owing to the numerous interactions involved. For example, it might seem to be unsurprising that **7b** is computed to be less well bound than **7a** since there is no water in the pocket for a hydrogen bond with the indole NH of **7b**. However, the indole NH of **7a** is also not able to participate in a hydrogen bond and the favorability of the electrostatic interactions with Trp229 and Tyr188 are unclear. The methylated **7c** does bind better than **7b** since the methyl group is placed in the pocket, though whether or not there is enough room is unclear without the result. The strong preference for the indolizine **7d** over its isomer **7e** is striking and must reflect electrostatic differences, which have arisen before for indolizine derivatives.[21] Similarly, **7g** is preferred over **7f**. Furans are very poor hydrogen-bond acceptors, so the pattern is that it is beneficial to have a more acidic (positive) hydrogen near the tryptophan ring (**7a, 7d, 7g**) than a more electron rich atom. Continuing, introduction of a nitrogen atom at C2 of the 5-membered ring turned out to be detrimental in each case, **7h** – **7k**, by ca. 3 kcal/mol. In the MC simulations it is found that water in the tunnel does not penetrate past the Phe227-Trp229 loop, so a hydrogen bond with water is not made to the 2-position nitrogen atom. Thus, it appears that a cyano group at this position is needed to reach a water molecule in the tunnel.

Finally, the results for introduction of a methyl group at C2 to yield **7l** – **7r** were interesting. In some cases, there is significant benefit, e.g., **7a** going to **7l**, while in others there is little change (**7e** to **7p**, or **7g** to **7r**). In analyzing this, it appears that a key factor is the angle of projection of the methyl group into the tunnel. For **7l** in the snapshot in Figure 2 the NH-C2-CH_3 bond angle is 116° and the methyl group is directed upward above C_α of Phe227. The corresponding angle (C3-C2-CH_3) in snapshots for **7m** is near 130°, which brings the methyl group too close to the C_α atom. When 2-methylindole is optimized with OPLS/CM1A the corresponding angles are 120.1° and 130.2°. With *ab initio* calculations at the HF/6–311G(d) level the results are 120.6° and 130.2°, and with MP2/6-311G(d) optimizations they are 121.0° and 130.5°.[22] For 2-methylbenzofuran, the O-C2-CH_3 and C3-C2-CH_3 angles are computed to be 118.3° and 129.7° with OPLS/CM1A. Thus, **7f** benefits from addition of the methyl group in going to **7q**, while the addition of the methyl group to **7g** to give **7r** is predicted to reduce the binding affinity. This reverses the preference for **7g** over **7f**.

SYNTHETIC CHEMISTRY

Based on the MC/FEP results in Figure 1, the synthetic efforts were directed at substituted indoles, indolizines, and benzofurans corresponding to **8, 10**, and **12**. A few of the isomers **9, 11**, and **13** were also prepared. The full list of analogs that were synthesized is given in Table 1. While complete synthetic details and compound characterization are provided in the Supplementary Information, the synthetic routes for the key compounds with a cyano group in the 2-position of the bicyclic heterocycle are summarized here. The identity of all

compounds was confirmed by ^{1}H and ^{13}C NMR and high-resolution mass spectrometry; purity was >95% as judged by high-performance liquid chromatography.

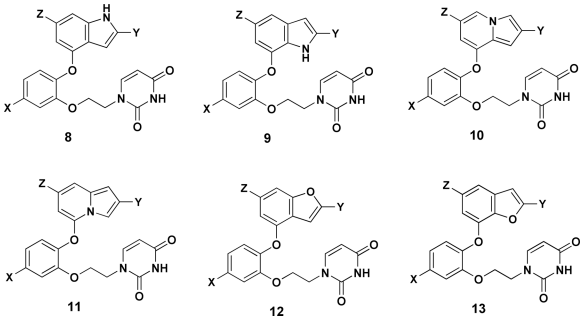

For the 2-cyanoindoles **8** (Y = CN), the pathway is illustrated in Scheme 1. The syntheses began with an S_NAr reaction between a 2-fluorobenzaldehyde and a 2-benzyloxyphenol to yield the phenoxybenzaldehyde scaffold.[23] Cyclization to the indole was achieved using methyl azidoacetate,[24] which was followed by reduction of the ester to the alcohol, and then oxidation to the aldehyde.[25] After conversion of the aldehyde at C2 to the desired nitrile[26] and Boc-protection of the indole nitrogen, the benzyl group was cleaved. To install the uracil containing side chain, the phenol was unmasked and alkylated with 3-benzoyl,1-bromoethyluracil. Finally, the Boc group was removed with tetra-*n*-butylammonium fluoride, and the uracil moiety was deprotected under basic conditions to afford the desired products. It may be noted that alternatives to the Boc-protection were considered via addition of methyl chloroformate or triisopropylsilyl chloride; however, in these cases, the deprotection step proved difficult.

For the indolizines **10** (Y = CN), comparatively easy installation of the desired cyano group at the 2-position was possible using acrylonitrile in the cyclization sequence,[27] as summarized in Scheme 2. The resultant 8-bromo-2-cyanoindolizines underwent an S_NAr reaction with a substituted 2-methoxyphenol to yield the diarylethers. Installation of the uracilylethoxy side chain then proceeded as in Scheme 1, following demethylation of the methoxy group with BBr_3. The starting picolinaldehydes were obtained either by DIBALH reduction of the corresponding 2-methylester or SeO_2 oxidation of the 2-methyl analog when Z was chlorine.

For the 2-cyanobenzofurans **12** (Y = CN), the synthetic route in Scheme 3 begins with conversion of 2-hydroxybenzaldehyde derivatives to dibromovinyphenols using tetrabromomethane and triphenylphosphine (Scheme 3). A ligand-free, copper-catalyzed cross-coupling ensued to yield substituted 2-bromobenzofurans,[28] which was followed by selective displacement of the 2-bromine with sodium cyanide to yield 2-cyanobenzofurans. The rest of the sequence then proceeded as for the 2-cyanoindolizines. Access to the starting aldehydes was more involved in this case requiring a five step procedure beginning with commercially available 2-bromo-6-methoxyanilines, as detailed in the Supplementary Information.

ASSAY RESULTS

As in previous studies,[6,9,14] activities against the IIIB strain of HIV-1 were measured using human MT-2 T-cells; EC_{50} values are obtained as the dose required to achieve 50% protection of the infected cells by the MTT colorimetric method.[29,30] Activities against variant strains of the virus, which contain the clinically important Y181C and K103N/Y181C mutations in the RT enzyme, were also determined. CC_{50} values for inhibition of MT-2 cell growth by 50% are obtained simultaneously. The antiviral and toxicity curves

used triplicate samples at each concentration. The results including those for several reference NNRTIs are listed in Table1.

The results for activity towards the wild-type virus are discussed first. The parent indole **8a** turned out to be an 85-nM inhibitor, which is more potent than the drug nevirapine. Addition of a chlorine at C5 in the phenyl ring (**8b**) and of a 2-methyl group in the bicycle (**8c**) were not beneficial; however, the 2-cyano analog **8d** did provide an improvement to 56 nM. Elaboration with a methyl group at the 6-position to yield **8e** yielded a 10-nM NNRTI, while a chlorine at this position (**8f**) reduced the potency to 340 nM. Increased steric sensitivity is indicated in the pocket near Pro95 (Figure 2) compared to the case with the cyanovinylphenyl-containing catechol diethers,[9] which would be consistent with the greater rigidity of the bicyclic alternatives. Only two of the isomeric indoles, **9a** and **9b**, were prepared. **9b**, the isomer of **8c**, was inactive, which is qualitatively consistent with the expectations from the MC/FEP results for **7l** and **7m** in Figure 1. For **9a**, comparison can be made with **8a**; the added methyl group reduces the activity ca. 70-fold, which is consistent with the predictions for **7a** and **7m** in Figure 1. In general, quantitative agreement is not expected between the MC/FEP results for relative free energies of binding and the EC_{50} results from the cell-based assays. Correct qualitative guidance is all that is needed for great facilitation of lead optimization.

The first two indolizines that were synthesized were **10a** and **10b**. The 2-cyano analog **10b** was extremely potent at 0.38 nM (380 pM) and more than 100-fold more so than the methyl analog **10a. 10b** also showed no cytotoxicity (CC_{50}) up to the maximum tested concentration, 100 μM. This demonstrates that the design strategy of replacing the cyanovinylphenyl substituent could be very successful with proper choice of a cyano-substituted bicyclic heterocycle. A substituent in the 6-position of the indolizine was then explored with **10c** – **10e**. The methyl and fluoro derivatives, **10c** and **10d**, are high picomolar inhibitors, while the Z = Cl analog **10e** was again less potent at 3.7 nM. Among the remaining indolizines, the difluoro compound **10h** was the most potent with an EC_{50} of 0.4 nM; it also shows low cytotoxicity with a CC_{50} of 50 μM. Placement of a fluorine at C4 in the phenyl ring yielded **10j**, which was found to have similar potency as the 5-fluoro analog, **10f**. However, there was no added benefit of having fluorines at both C4 and C5 (**10k, 10l**). Only one isomeric indolizine was prepared, **11a**. Consistent with the FEP results, it is less active than its isomer **10f**, though the 6-fold difference is smaller than what might be expected from the results in Figure 1. This may stem from the computations being for the methyl (**7o, 7p**) rather than cyano compounds and/or limitations with the point-charge model in the force field and its accounting of the aryl-aryl interactions with Tyr181, Tyr188, and Trp229 (Figure 2).

The focus on the benzofurans was also for the 2-cyano substituted cases. The parent **12a** emerged as an 18-nM inhibitor. Addition of the 6-methyl group to give **12b** was now significantly detrimental (210 nM), while a chlorine at this position (**12c**) had no impact. For the fluoro analogs, **12d** and **12e**, addition of the 6-methyl group is again detrimental, and for the chloro compounds **12f** – **12g** the 100-fold benefit of progressing from hydrogen to methyl to cyano at the 2-position is apparent. Only one isomeric benzofuran **13a** was prepared. Based onthe FEP results in Figure 1, a strong preference for the **12** series over **13** was not expected. However, the qualitative order is correct for the one case of **13a** versus its isomer **12f**. Overall, the FEP results were highly successful in narrowing the field of possible synthetic targets and in leading the discovery of the strikingly potent indolizines, especially **10b** and **10h**.

The performance of the compounds towards the mutant strains of HIV-1 is also recorded in Table 1. The variations in the results are difficult to rationalize with confidence in the

absence of more experimental structural characterization of the complexes. However, the general pattern is that compounds that are more potent towards the wild type virus are also more potent towards the variants. Furthermore, the usual pattern with NNRTIs is that they are more potent towards the single Y181C variant than the double K103N/Y181C variant. Both variants are clinically important and the double mutant is viewed as being the most challenging variant. The K103N mutation is found in 57% of cases of NNRTI resistance and Y181C is found in 25% of cases.[31] Thus, it was surprising to find that the new compounds are almost uniformly more active towards the K103N/Y181C than the Y181C variant. The EC_{50} values of 11 and 10 nM for **10b** and **10h** with the double variant are impressive and represent significant improvement over the results for **3** and **4**. However, **3** and **4** perform ca. 10-fold better for the single mutant. Among the new compounds the greatest potency towards the Y181C variant is for **10d** and **10i** at 170 and 160 nM. It is easy to say that the present compounds are expected to lose potency towards Y181C variants owing to loss of aryl-aryl contacts indicated in Figure 2 and in the crystal structures for the complexes of **3** and **4**.[10] However, the reason for the greater loss for **10b** and **10h** is unclear, and the reason for the gain in activity for adding the K103N mutation is especially obscure.

CRYSTALLOGRAPHY

In order to begin to obtain a deeper understanding of the variations in activity for the indolizines, an X-ray crystal structure for **10b** with WT HIV-1 RT was determined in the same manner as for **3** and **4**.[10] The best crystals obtained using the recombinant RT52A enzyme diffracted to amplitudes extending to 2.88 Å, and phases were determined via molecular replacement using the structure for **3** as the search model (PDB code: 4H4M).[10] The overall conformation of the binding pocket is similar to the 4H4M structure in which the β*6*-β*10*-β*9* sheet (p66: residues 105–110, 186–191, 178–183, respectively) and YMDD loop (p66: residues 183–186) shift in order to interact with the bound inhibitor. The crystal structure for the complex with **10b** is illustrated in Figure 3; the positioning of the ligand and the contacts are predominantly as expected from Figure 2 with the cyano group projecting into the tunnel behind Phe227. An all-atom alignment comparing the inhibitor and non-nucleoside binding pocket of the 4H4M structure and the **10b**:RT complex gives an rmsd of only 0.75 Å.

In the computer simulations and the crystal structure for **3** and **10b** there is some variation in the conformation of the uracilylethoxy group where the dihedral angle for the connection to the central phenyl ring (C2-C1-O-C) can either be near 180° (*anti* as in Figure 3) or nearer *syn* as in the case for **3**.[10] The change is accompanied by some differences in hydrogen bonding between the uracil ring and Lys102, Lys103, and Pro236. In the present case, the C2 carbonyl oxygen of the uracil is 3.1 Å from the backbone N of Lys103, and N3 of the uracil is 3.4 Å from the backbone carbonyl oxygen of Pro236. However, the latter pair is not oriented well for hydrogen bonding, as illustrated in Figure 4. This region is solvent exposed and significant exchange of protein-ligand, protein-water, and ligand-water hydrogen bonds is observed in the MC simulations.

There are additional points of note. The orientation of Tyr181 is the same in Figure 2 and Figure 3 with the tyrosine ring and the central ring of the inhibitor perpendicular, while in the crystal structures for **3** and **4** they are parallel owing to 90° rotation of the tyrosine ring. In both cases the interaction is offset so it is not an optimal aryl-aryl interaction. However, the edge-to-face interaction between Tyr181 and the indolizine 6-membered ring of **10b** does appear to be ideal and is such that a substituent could not be placed at C6 of the indolizine (Z in **10**) without steric conflict with the tyrosine ring. The tight packing is apparent in Figure 4. It seems likely that placement of a substituent at C6 would be accompanied by rotation of the tyrosine ring to the parallel geometry observed for the

complexes of **3** and **4**. Thus, the adverse effects of the Tyr181Cys mutation on potency for the indolizines can be attributed primarily to the loss of the aryl-aryl interaction between the bicyclic heterocycle and Tyr181.

Turning to Lys103, the orientation of its side chain is the same in the three crystal structures and from the MC modeling of the complexes. The side chain extends into the entrance channel of the NNRTI binding site with the ammonium group solvent exposed (Figure 3 and Figure 4). The shortest contact between the side chain and the inhibitors is between C_β and C5 in the central ring at 3.8 to 4.1 Å separation. A substituent on C5 (X in **8** – **13**) would also be in van der Waals contact with C_β of Lys103. It is unclear based on the present structures why conversion of Lys103 to Asn is beneficial for the heterobicyclic catechol diethers and not so for the cyanovinylphenyl analogs. Crystal structures for additional complexes such as for **3** and **10b** with Y181C, K103N, and K103N/Y181C HIV-RT are much desired to provide clarification.

A final structural point concerns the positioning of the cyano groups of the inhibitors in the tunnel. Figure 5 provides two views comparing the crystal structures for **3** and **10b**. They show that there are some differences such that the indolizine makes closer contact with Trp229 and that the cyano group of **3** extends further into the tunnel. As a result the cyano nitrogen atom of **3** is only 3.6 Å from the ammonium nitrogen of Lys223 (Figure 5b), while the corresponding distance in the complex for **10b** is 5.8 Å. In the crystal structure for **4**, the side chain of Lys223 has a conformational kink that increases the separation to 6.5 Å (PDB code: 4H4O). There is water in this region that promotes the variety of possible arrangements. In any event, ion-dipole interactions with Lys223 or direct hydrogen bonding to water or Lys223 are expected to be contributing to the observed strong benefits of the cyano groups to the antiviral activity.

SOLUBILITY

Poor solubility, which has been a problem for many NNRTIs, often leads too low bioavailability, difficulties in formulation, and high dosages.[6,32,33] The issue reflects the hydrophobic nature of the NNRTI binding site. In the design of the catechol diethers, attention was paid to having both good potency and aqueous solubility. In our laboratory, solubilities are measured using a shake-flask procedure.[6,34] The compounds are dissolved in Britton-Robinson buffer and stirred in vials for 48 hours at 25 °C. The pH of the buffer solutions is 6.5 as measured by a Corning General Purpose pH Combination probe (4136L21). The solution containing excess solid is filtered using a Whatman Mini-UniPrep syringeless filter device with a 0.45 μm pore size, and the supernatant is analyzed by UV-vis spectrophotometry (Agilent 8453).

As shown in Table 2, the solubilities for the drugs etravirine and rilpivirine are below 1 μg/ml, which is well outside the normal range of 4 – 4000 μg/ml for oral drugs.[6,33] The solubilities of the most potent indolizine analogs, **10b** and **10h**, are both ca. 40 μg/ml. **4**, the cyanovinylphenyl analog of **10h**, is 4-fold less soluble at 11 μg/ml. As also shown in Table 2, there is reasonable inverse correlation of the observed solubilities with computed octanol-water partition coefficients, which are readily obtained using ChemDraw.[38] Thus, it was expected that the new compounds would have solubilities somewhat less than for nevirapine, but much greater than for etravirine or rilpivirine.

CONCLUSION

Computer simulations guided the discovery of potent, novel inhibitors of HIV-1 reverse transcriptase. MC/FEP calculations were used to analyze possible replacements for a

cyanovinylphenyl group that has been featured in prior NNRTIs, but that possesses reactivity concerns. The results indicated that indoles, indolizines, and benzofurans as represented by **8, 10**, and **12** would be the most viable. The predictions were validated by synthesis and assaying that yielded inhibitors of the wild-type virus with EC_{50} values of 10 nM or lower in all three series. The most active compounds are the indolizines **10b** and **10h** which are strikingly potent with EC_{50} values of 0.4 nM towards the wild-type virus and 10 nM towards a difficult variant strain bearing K103N and Y181C mutations in the RT enzyme. The structural characterization was much enhanced by obtaining an X-ray crystal structure for **10b** in complex with HIV-RT at 2.88-Å resolution. The structure confirmed the expected placement of the inhibitor in the binding site, the extensive aryl-aryl interactions with Tyr181, Tyr188, and Trp229, and the extension of the cyano group of **10b** towards Lys223 in the tunnel region. The contact between Tyr181 and the C6-C7 region of the indolizine appears to be optimal and can explain the significant loss in activity of **10b** and **10h** towards the Y181C variant. However, the structural origin of the ca. 30fold gain in activity upon addition of the K103N mutation is unclear and makes further crystallographic investigation desirable. The aqueous solubilities of **10b** and **10h** were also measured and, at ca. 40 μg/ml, they are in the normal range for oral drugs. In comparison to the FDA-approved drug efavirenz, **10b** and **10h** show improved activity towards the wild-type virus and the K103N/Y181C variant, diminished activity towards the Y181C variant, lower cytotoxicity, and similar solubility. In comparison to etravirine and rilpivirine, the new NNRTIs show similar activity towards the wild-type virus and the K103N/Y181C variant, poorer activity towards the Y181C variant, reduced cytotoxicity, and at least 100-fold greater solubility. Overall, the valuable role that FEP calculations can play in lead optimization has been further illustrated,[7] equivalents for a cyanovinylphenyl group have been reported, and novel, potent anti-HIV agents with low cytotoxicity and good solubility have been discovered and structurally characterized.

Supplementary Material

Refer to Web version on PubMed Central for supplementary material.

Acknowledgments

Gratitude is expressed to the National Institutes of Health (AI44616, GM32136, GM49551) for research support and for a fellowship to KMF (AI104334). Dr. Xiaoling Wu is thanked for assistance with the NMR spectroscopy. Receipt of the following reagents through the NIH AIDS Research and Reference Reagent Program, Division of AIDS, NIAID, NIH is also greatly appreciated: MT-2 cells, catalog #237, and nevirapine-resistant HIV-1 (N119), catalog #1392, from Dr. Douglas Richman; HTLV-III_B/H9, #398, from Dr. Robert Gallo; and HIV-1_{IIIB} (A17 Variant) from Dr. Emilio Emini.

REFERENCES

1. Asahchop EL, Wainberg MA, Sloan RD, Tremblay CL. Antimicrob. Agents Chemother. 2012; 56:5000–5008. [PubMed: 22733071]
2. Zhan P, Chen X, Li D, Fang Z, De Clercq E, Liu X. Med. Res. Rev. 2013; 33(S1):E1–E72. [PubMed: 21523792]
3. Permpalung N, Putcharoen O, Avihingsanon A, Ruxrungtham K. Expert Opin. Pharmacother. 2012; 13:2301–2317. [PubMed: 23043453]
4. James C, Preininger L, Sweet M. Am. J. Health-Syst. Pharm. 2012; 69:857–861. [PubMed: 22555080]
5. Janssen PAJ, Lewi PJ, Arnold E, Daeyaert F, de Jonge M, Heeres J, Koymans L, Vinkers M, Guillemont J, Pasquier E, Kukla M, Ludovici D, Andries K, de Bethune M-P, Pauwels R, Das K, Clark AD Jr. Frenkel YV, Hughes SH, Medaer B, De Knaep F, Bohets H, De Clerck F, Lampo A, Williams P, Stoffels P. J. Med. Chem. 2005; 48:1901–1919. [PubMed: 15771434]

6. Bollini M, Cisneros JA, Spasov KA, Anderson KS, Jorgensen WL. Bioorg. Med. Chem. Lett. 2013; 23:5213–5216. [PubMed: 23937980]
7. Jorgensen WL. Acc. Chem. Res. 2009; 42:724–733. [PubMed: 19317443]
8. Stepan AF, Walker DP, Bauman J, Price DA, Baillie TA, Kalgutkar AS, Aleo MD. Chem. Res. Toxicol. 2011; 24:1345–1410. [PubMed: 21702456]
9. Bollini M, Domaoal RA, Thakur VV, Gallardo-Macias R, Spasov KA, Anderson KA, Jorgensen WL. J. Med. Chem. 2011; 54:8582–8591. [PubMed: 22081993]
10. Frey KM, Bollini M, Mislak AC, Cisneros JA, Gallardo-Macias R, Jorgensen WL, Anderson KA. J. Am. Chem. Soc. 2012; 134:19501–19503. [PubMed: 23163887]
11. Fleming FF, Wang Q. Chem. Rev. 2003; 103:2035–2077. [PubMed: 12744700]
12. Dahlgren MK, Schyman P, Tirado-Rives J, Jorgensen WL. J. Chem. Inf. Model. 2013; 53:1191–1199. [PubMed: 23621692]
13. Fleming FF, Yao L, Ravikumar PC, Funk L, Shook BC. J. Med. Chem. 2010; 53:7902–7917. [PubMed: 20804202]
14. Jorgensen WL, Bollini M, Thakur VV, Domaoal RA, Spasov K, Anderson KS. J. Am. Chem. Soc. 2011; 133:15686–15696. [PubMed: 21853995]
15. Jorgensen WL, Tirado-Rives J. J. Comput. Chem. 2005; 26:1689–1700. [PubMed: 16200637]
16. Jorgensen WL, Maxwell DS, Tirado-Rives J. J. Am. Chem .Soc. 1996; 118:11225–11236.
17. Jorgensen WL, Tirado-Rives J. Proc. Natl. Acad. Sci. U.S.A. 2005; 102:6665–6670. [PubMed: 15870211]
18. Jorgensen WL, Chandrasekhar J, Madura JD, Impey RW, Klein ML. J. Chem. Phys. 1983; 79:926–935.
19. for a review, see. Jorgensen WL, Thomas LT. J. Chem. Theory Comput. 2008; 4:869–876. [PubMed: 19936324]
20. Heugebaert TSA, Roman BI, Sevens CV. Chem Soc. Rev. 2012; 41:5626–5640. [PubMed: 22782188]
21. Kim JT, Hamilton AD, Bailey CM, Domaoal RA, Wang L, Anderson KS, Jorgensen WL. J. Am. Chem. Soc. 2006; 128:15372–15373. [PubMed: 17131993]
22. Frisch, MJ. Gaussian 09, Revision A.02. Wallingford, CT: Gaussian, Inc; 2009. [Full reference is given in the Supporting Information.]
23. Whitlock GA, Blagg J, Fish PV. Bioorg. Med. Chem. Lett. 2008; 18:596–599. [PubMed: 18240382]
24. Bamberg JT, O'Yang C, Sui M, Zhao S-H. 2010 US7741326 B2.
25. Zheng C, Lu Y, Zhang J, Chen X, Chai Z, Ma W, Zhao G. Chem. Eur. J. 2010; 16:5853–5857. [PubMed: 20391582]
26. (a) Ryabova SY, Alekseeva LM, Lisitsa EA, Granik VG. Russ. Chem. Bull., Int. Ed. 2006; 55:1248–1254.(b) Attanasi O, Palma P, Serra-Zanetti F. Synthesis. 1983; 9:741–742.
27. Bode ML, Kaye PT. J. Chem. Soc. Perkin Trans. 1993; 1:1809–1813.
28. (a) Newman SG, Aureggi V, Bryan CS, Lautens M. Chem. Commun. 2009:5236–5238.(b) Zhou W, Chen W, Wang L. Org. Biomol. Chem. 2012; 10:4172–4178. [PubMed: 22538559]
29. Lin TS, Luo MZ, Liu MC, Pai SB, Dutschman GE, Cheng YC. Biochem. Pharmacol. 1994; 47:171–174. [PubMed: 8304960]
30. Ray AS, Yang Z, Chu CK, Anderson KS. Antimicrob. Agents Chemother. 2002; 46:887–891. [PubMed: 11850281]
31. de Béthune M-P. Antiviral Res. 2010; 85:75–90. [PubMed: 19781578]
32. Lipinski CA, Lombardo F, Dominy BW, Feeney PJ. Adv. Drug Deliv. Rev. 2001; 46:3–26. [PubMed: 11259830]
33. Jorgensen WL, Duffy EM. Adv. Drug Deliv. Rev. 2002; 54:355–366. [PubMed: 11922952]
34. Baka E, Comer JEA, Takács-Novák K. J. Pharm. Biomed. Anal. 2008; 46:335–341. [PubMed: 18055153]
35. Morelock MM, Choi LL, Bell GL, Wright JL. J. Pharm. Sci. 1994; 83:948–952. [PubMed: 7525921]

36. Weuts I, Van Dycke F, Voorspoels J, de Cort S, Stokbroekx S, Leemans R, Brewster ME, Xu D, Segmuller B, Turner YTA, Roberts CJ, Davies MC, Qi S, Craig DQM, Reading M. J. Pharm. Sci. 2011; 100:260–274. [PubMed: 20575005]

37. Sun L-Q, Qin B, Huang L, Qian K, Chen C-H, Lee K-H, Xie L. Bioorg. Med. Chem. Lett. 2012; 22:2376–2379. [PubMed: 22406117]

38. ChemDraw. CambridgeSoft Inc.: Cambridge, MA; 2013.

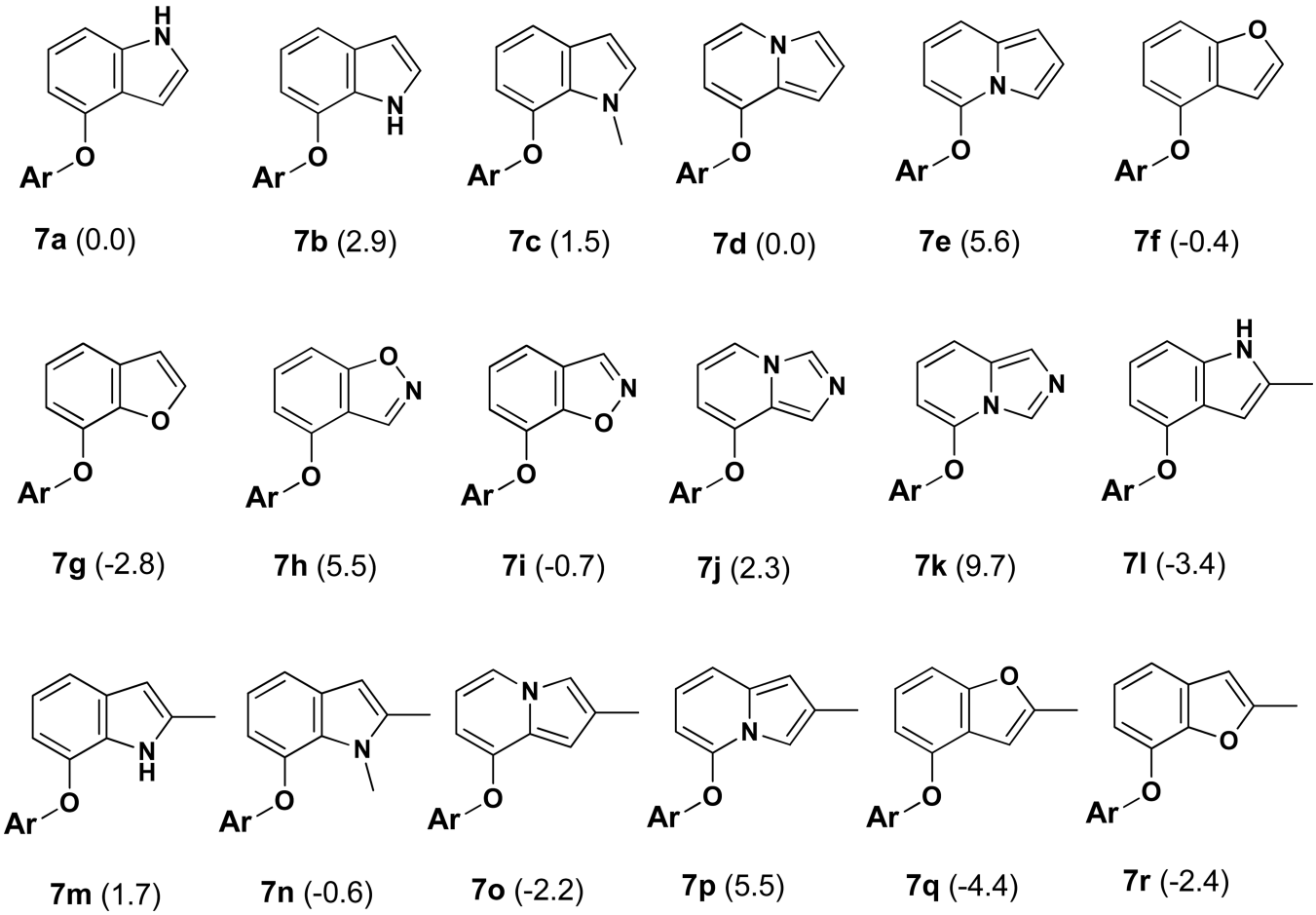

Figure 1.

Modeled compounds where Ar is the uracilylethoxyphenyl substructure of **5** or **6** with R' = Cl. The number in parentheses is the computed relative free energy of binding (kcal/mol) with HIV-RT from the FEP calculations; the statistical uncertainty in the results is ±0.5 kcal/mol.

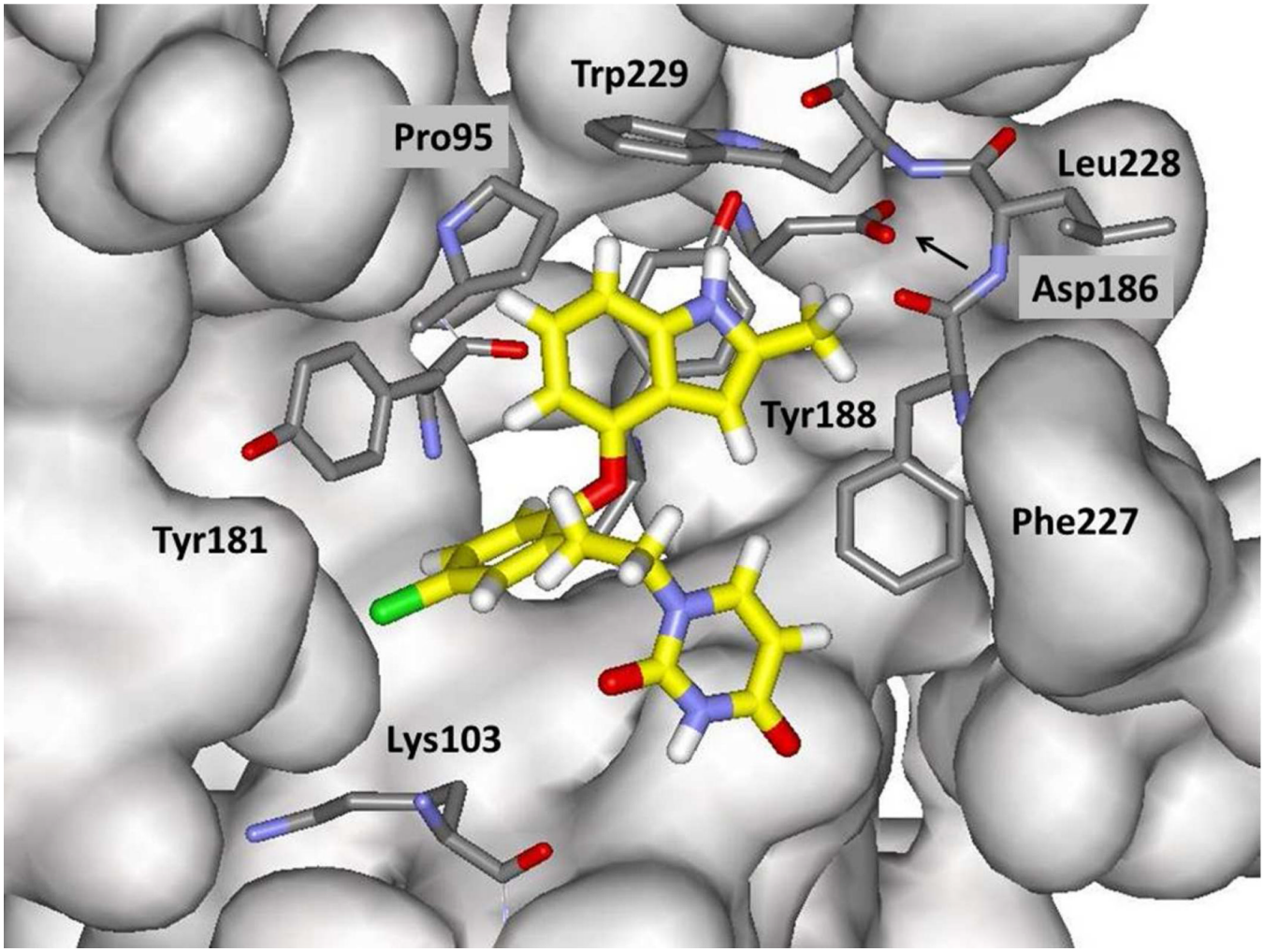

Figure 2.
Illustration of a configuration from an MC simulation of the indole **7l** bound to wild type HIV-1 reverse transcriptase. Carbon atoms of **7l** are rendered in yellow. All water molecules and many residues in front of the ligand have been removed for clarity.

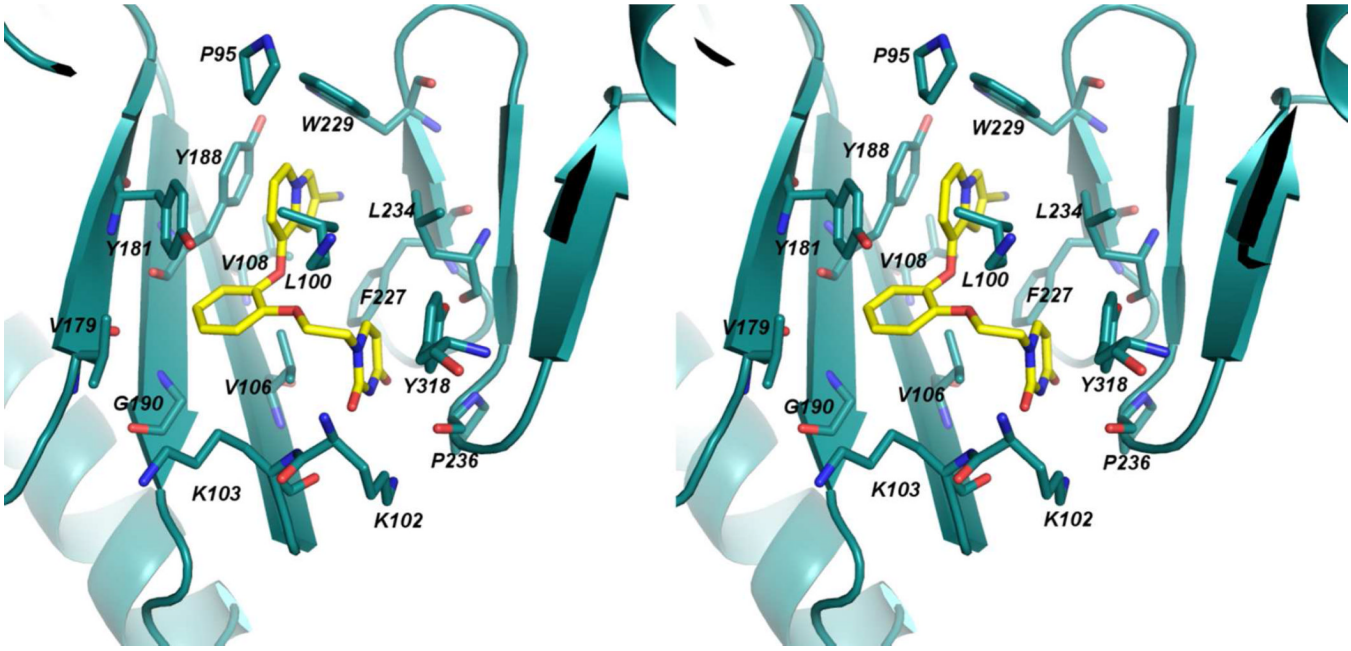

Figure 3.
Stereo view of the crystal structure for **10b** complexed with HIV-RT. Numerous contacts in the binding site are apparent and consistent with those in the crystal structures for **3** and **4** and in the modeled structure in Figure 2. The PDB code is 4MFB.

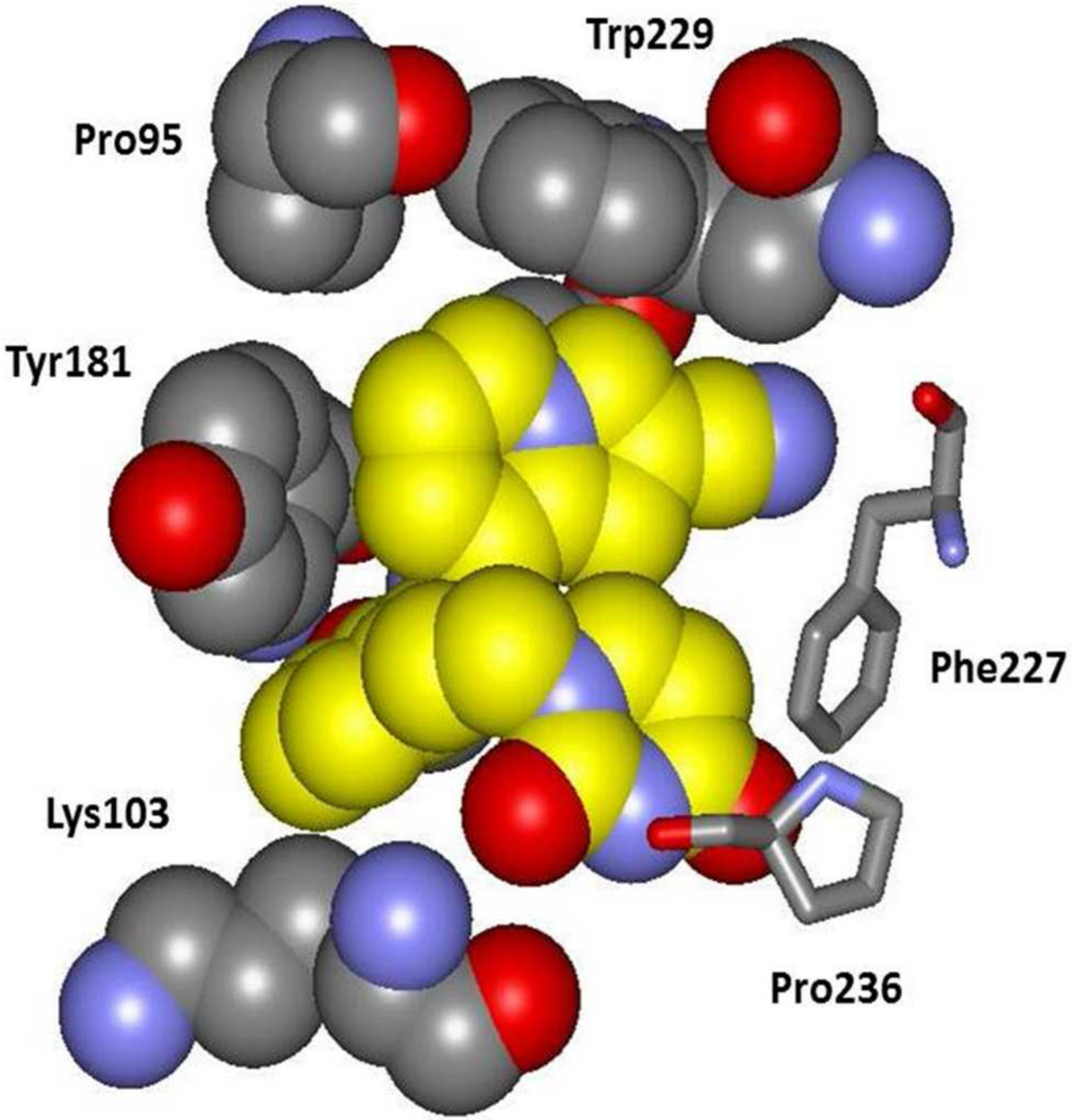

Figure 4.

A space-filling rendering made from the crystal structure of **10b** bound to HV-RT. Carbon atoms of **10b** are in yellow. Notable points are the hydrogen bond between a uracil oxygen atom and the backbone NH of Lys103, the aryl-aryl contacts with Tyr181 and Trp229, and the orientation of Lys103 including the contact of the C_β atom with the inhibitor.

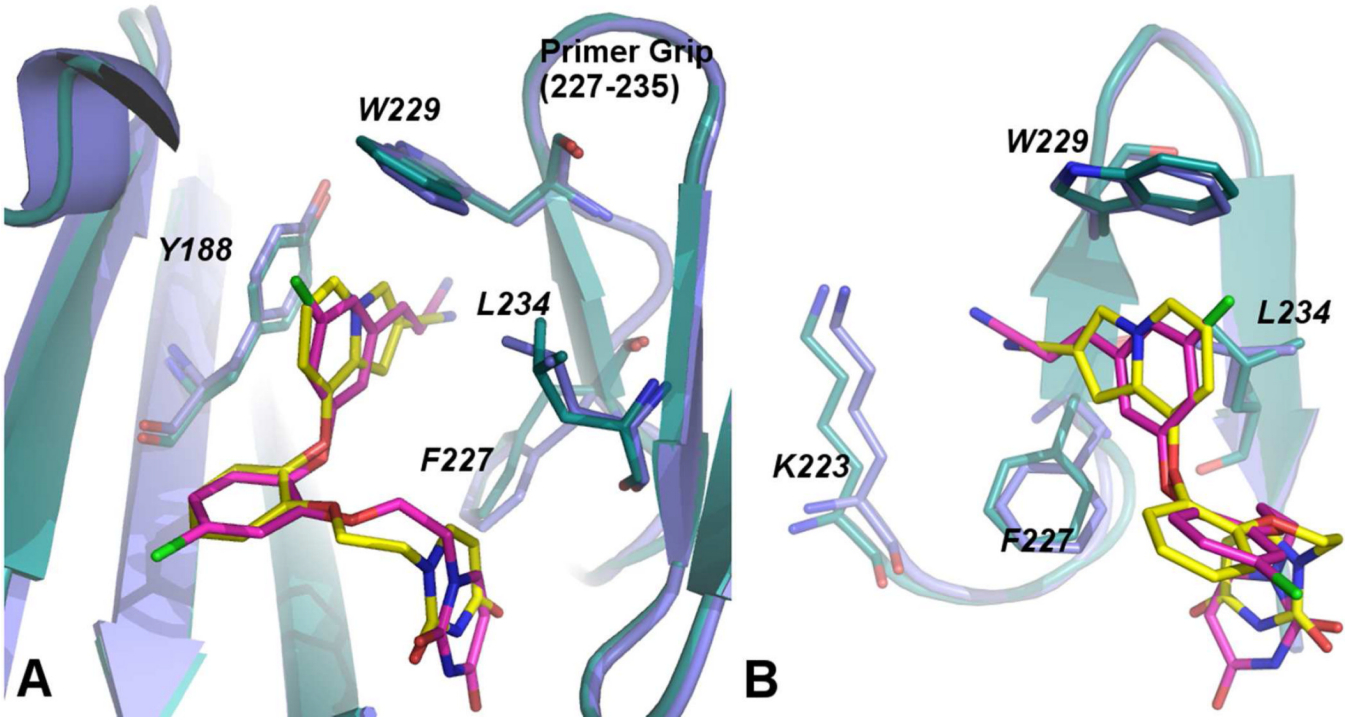

Figure 5.
Two views comparing the crystal structures for **3** and **10b**. In A, the difference in conformation of the uracilylethoxy side chain is apparent, while B illustrates that the cyano group of **3** extends farther into the tunnel region and closer to Lys223.

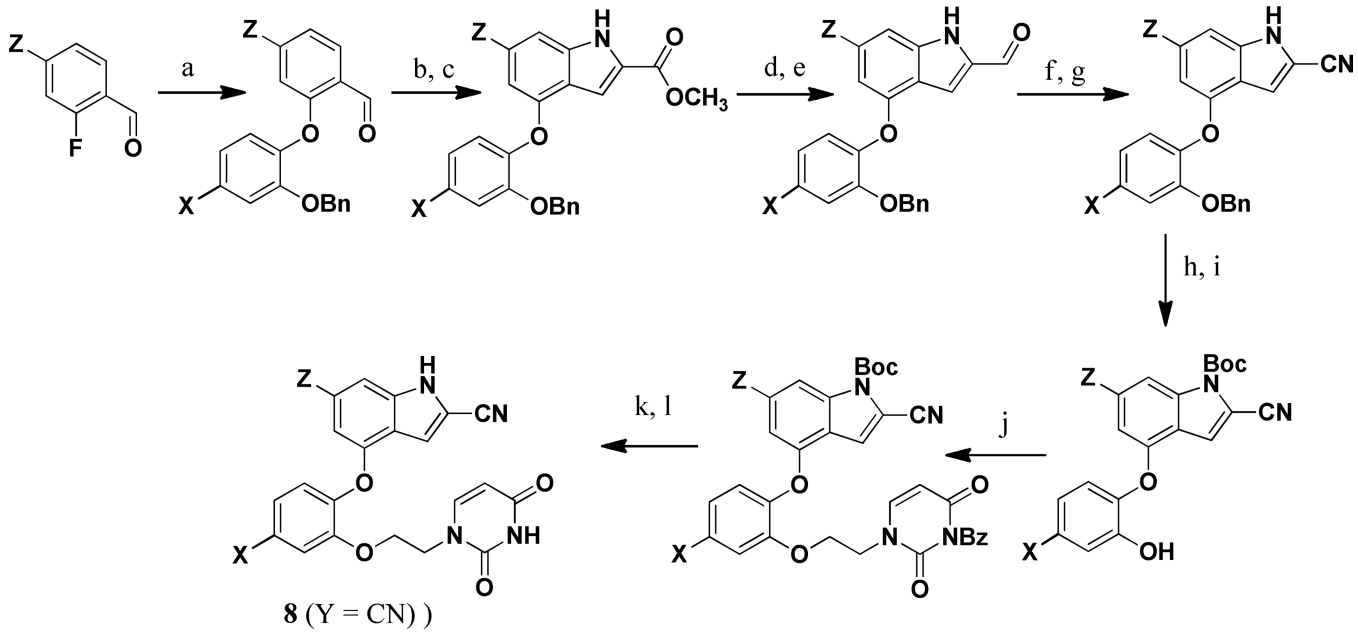

Scheme 1. Synthesis of the 2-Cyanoindoles

Reagents: (a) K_2CO_3, DMF, 100–120 °C, 12 h; (b) methyl azidoacetate, −40 °C, NaOMe, MeOH, 12 h; (c) xylene, reflux, 4 h; (d) LAH,THF, 0 °C, 0.5 h; (e) MnO_2, DCM, rt, 24 h; (f) NH_2 OSO_3 H, MeOH, reflux, 0.5 h; (g) $Cu(OAc)_2$, CH_3 CN, reflux, 1 h; (h) 4-DMAP, Boc_2O, THF, rt, 12 h; (i) H_2 /Pd/C, MeOH, rt, 0.5 h; (j) 3-benzoyl,1-bromoethyluracil, K_2CO_3, DMF, 60 °C, 2 h; (k) TBAF, THF, reflux, 24 h; (l) NH_3, MeOH, rt, 12 h.

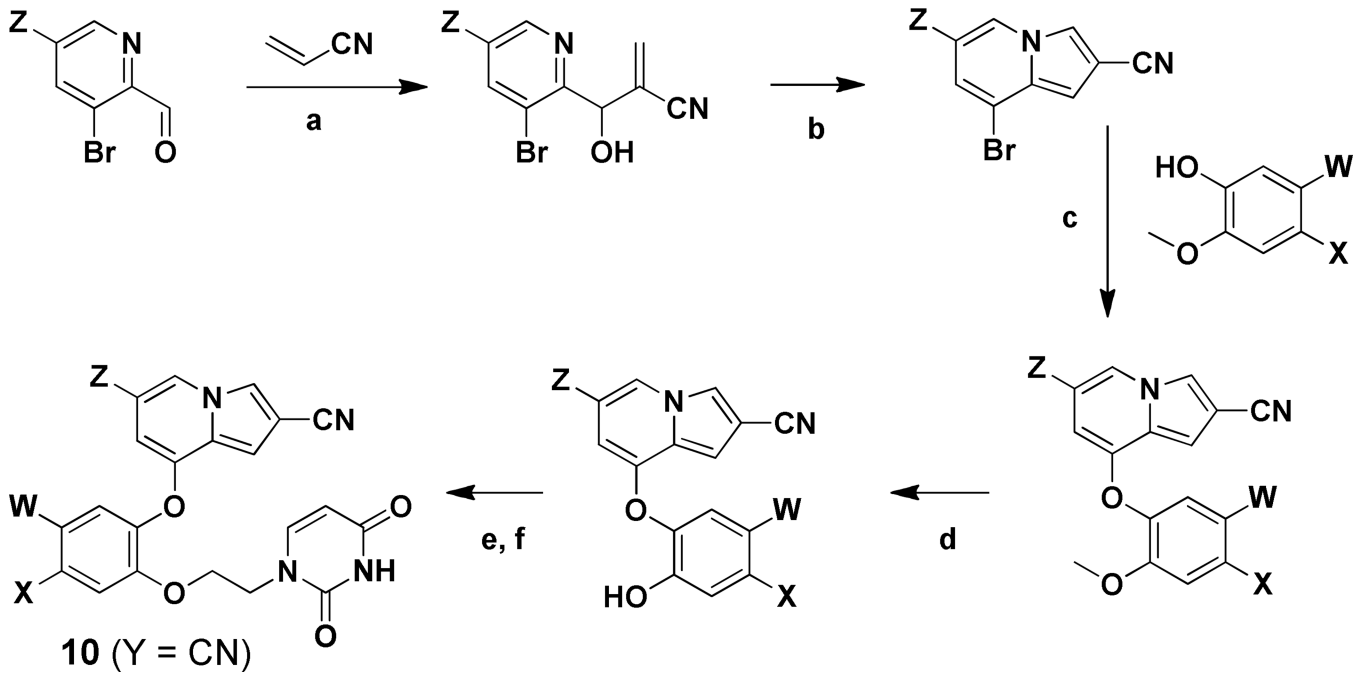

Scheme 2. Synthesis of the 2-Cyanoindolizines

Reagents: (a) DABCO, neat, 2 h; (b) Ac_2O, 100 °C, 2 h →140 °C, 16 h; (c) CuI, Cs_2CO_3, 2,2,6,6-tetramethyl-3,5-heptanedione, dioxane, 120 °C, 18 h; (d) BBr_3, DCM, −78 °C → 0 °C, 3 h; (e) 3-benzoyl,1-bromoethyluracil, Cs_2CO_3 or K_2CO_3, DMF, 60 °C, 3 h; (f) NH_4OH, DCM, 16 h.

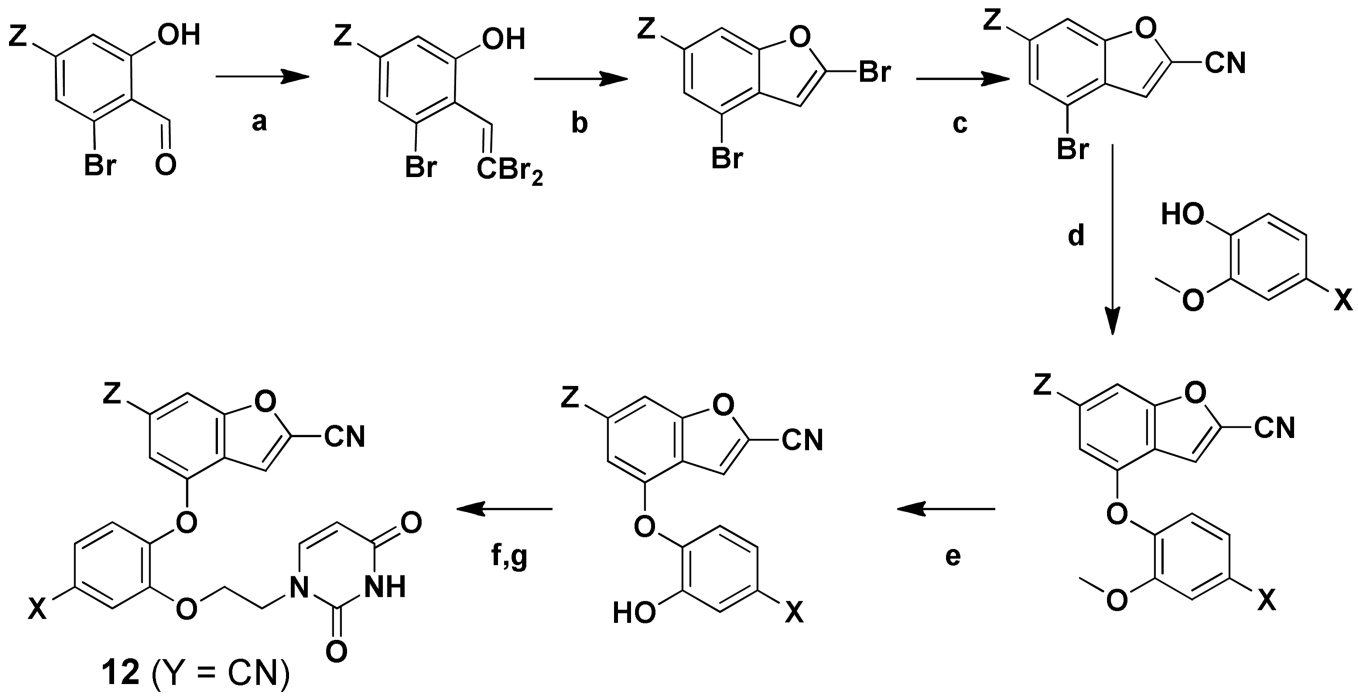

Scheme 3. Synthesis of the 2-Cyanobenzofurans

Reagents: (a) PPh_3, CBr_4, DCM, 0°C → RT, 2 h; (b) CuI, K_2CO_3, 80 °C, 4 h; (c) NaCN, DMSO, 100 °C, 24 h; (d) CuI, Cs_2CO_3*N*,*N*-dimethylglycine hydrochloride, dioxane, 90 °C, 18 h; (e) BBr_3, DCM, −78 °C → 0 °C, 3 h; (f) 3-benzoyl,1-bromoethyluracil, Cs_2CO_3 or K_2CO_3, DMF, 60 °C, 3 h; (g) NH_4OH, DCM, 16 h.

Table 1

Inhibitory Activity (EC_{50}) for HIV-1 and Cytotoxicity (CC_{50}) in μM

Compd	X	Y	Z	WT EC_{50}[a]	Y181C EC_{50}[a]	K103N/Y181C EC_{50}[a]	CC_{50}[b]
3				0.000055	0.049	0.220	10
4				0.00032	0.016	0.085	45
8a	H	H	H	0.085	ND	ND	53
8b	Cl	H	H	1.6	NA	NA	18
8c	H	CH_3	H	0.39	NA	NA	15
8d	H	CN	H	0.056	38	5.5	72
8e	H	CN	CH_3	0.010	NA	0.80	1.2
8f	H	CN	Cl	0.34	27	2.7	81
9a	H	H	CH_3	6.0	ND	ND	>100
9b	H	CH_3	H	NA	NA	NA	17
10a	H	CH_3	H	0.050	ND	ND	9.0
10b	H	CN	H	0.00038	0.31	0.011	>100
10c	H	CN	CH_3	0.00090	0.80	0.032	3.0
10d	H	CN	F	0.00070	0.17	0.068	40
10e	H	CN	Cl	0.0037	0.22	0.022	39
10f	F	CN	H	0.0027	0.60	0.22	100
10g	F	CN	CH_3	0.0020	0.40	0.25	17
10h	F	CN	F	0.00040	0.25	0.010	50
10i	F	CN	Cl	0.0025	0.16	0.11	15
10j	4-F	CN	H	0.0020	9.0	0.22	35
10k	4,5-diF	CN	H	0.0032	1.2	0.50	19
10l	4,5-diF	CN	F	0.0068	1.2	0.23	54
10m	Cl	CN	H	0.0051	1.8	0.90	55
10n	Cl	CN	Cl	0.022	0.41	0.53	20
11a	F	CN	H	0.017	6.9	1.3	>100
12a	H	CN	H	0.018	NA	0.42	>100
12b	H	CN	CH_3	0.21	NA	1.3	>100

Compd	X	Y	Z	WT EC_{50}[a]	Y181C EC_{50}[a]	K103N/Y181C EC_{50}[a]	CC_{50}[b]
12c	H	CN	Cl	0.019	1.9	0.26	>100
12d	F	CN	H	0.040	3.5	4.0	>100
12e	F	CN	CH_3	0.26	NA	5	>100
12f	Cl	H	H	0.800	ND	ND	19
12g	Cl	CH_3	H	0.025	NA	NA	8.0
12h	Cl	CN	H	0.0070	NA	NA	7.0
13a	Cl	H	H	0.900	ND	ND	50
nevirapine				0.11	NA	NA	>100
efavirenz				0.002	0.010	0.030	15
etravirine				0.001	0.008	0.005	11
rilpivirine				0.00067	0.00065	0.002	8

[a] For 50% protection in MT-2 cells; antiviral curves used triplicate samples at each concentration. ND for not measured. NA for $EC_{50} > CC_{50}$

[b] For 50% inhibition of MT-2 cell growth; toxicity curves also used triplicate samples.

J Am Chem Soc. Author manuscript; available in PMC 2014 November 06.

Table 2

Experimental Aqueous Solubility at pH 6.5 (S) and Computed ClogP

Compd	S, μg/mL	ClogP	Compd	S, μg/mL	ClogP
4	10.8	3.09	nevirapine	167[a]	2.65
10b	37.9	2.70	efavirenz	68.0	4.67
10h	43.8	3.14	etravirine	<< 1[b]	5.22
			rilpivirine	0.02,[c] 0.24[d]	5.75

[a] Ref. 35.

[b] Ref. 36.

[c] Ref. 5, pH 7.

[d] Ref. 37, pH 7.4.